Am J Transl Res 2026;18(1):498-511
www.ajtr.org /ISSN:1943-8141/AJTR0164622

Original Article

Cinnamaldehyde attenuates LPS-induced acute kidney injury by inhibiting ferroptosis via the Gsk3β/Nrf2/Gpx4 pathway

Wenjie Han[1*], Heng Sun[2*], Zhaomin Tian[3*], Yangyang Wang[5], Haitao Tian[1], Ye Tian[4]

[1]Department of Geriatric Medicine, The Sixth Medical Center of Chinese PLA General Hospital, Beijing 100048, China; [2]Senior Department of Oncology, The Fifth Medical Center of Chinese PLA General Hospital, Beijing 100039, China; [3]Orthopedics of TCM Clinical Unit, The Sixth Medical Center of Chinese PLA General Hospital, Beijing 100048, China; [4]Department of Anesthesiology, The Sixth Medical Center of Chinese PLA General Hospital, Beijing 100048, China; [5]Dapartment of Anesthesiology, Changzheng Hospital, Naval Military Medical University, Shanghai 200003, China. [*]Equal contributors.

Received March 18, 2025; Accepted September 22, 2025; Epub January 15, 2026; Published January 30, 2026

Abstract: Objectives: Sepsis-induced acute kidney injury (AKI) is a critical complication with limited treatment options. We investigated the protective effects of cinnamaldehyde (CA) on lipopolysaccharide (LPS)-induced AKI and elucidated underlying mechanisms focusing on ferroptosis and the glycogen synthase kinase 3 beta (GSK3β)/nuclear factor erythroid 2-related factor 2 (Nrf2)/glutathione peroxidase 4 (GPX4) pathway. Methods: Network pharmacology, molecular docking, and experimental validation were integrated. LPS-induced AKI models were established in C57BL/6 mice and human proximal tubular epithelial HK-2 (HK-2) cells. CA effects on renal function, histological injury, inflammation, and ferroptosis markers were evaluated. GSK3β involvement was tested via lentiviral overexpression. Protein and mRNA levels were measured by Western blotting, quantitative polymerase chain reaction (qPCR), enzyme-linked immunosorbent assay (ELISA), and immunofluorescence. Results: CA improved renal function and reduced tubular injury and inflammation. CA suppressed ferroptosis, evidenced by decreased malondialdehyde (MDA), iron, and lipid peroxidation, and normalization of GPX4 and acyl-CoA synthetase long chain family member 4 (ACSL4) expression. Network pharmacology and docking identified GSK3β as a key CA target; lentiviral GSK3β overexpression abolished CA's renoprotective and anti-ferroptotic effects. Mechanistically, CA activated Nrf2 and increased GPX4 expression via inhibition of the GSK3β/Nrf2/Kelch-like ECH-associated protein 1 (KEAP1) pathway. Conclusions: CA protects against LPS-induced AKI by inhibiting ferroptosis through modulation of the GSK3β/Nrf2/GPX4 axis, highlighting CA as a potential ferroptosis-targeted therapeutic candidate for septic AKI.

Keywords: Cinnamaldehyde, acute kidney injury, ferroptosis, sepsis

Introduction

Sepsis, a systemic inflammatory response syndrome triggered by bacteria, viruses, or fungi, can lead to severe consequences such as shock, multiple organ dysfunction syndrome (MODS), and ultimately, death [1]. Acute kidney injury (AKI) is one of the most common and severe complications, characterized by an abrupt decline in renal function and diagnosed primarily by elevated serum creatinine (Scr) levels or the presence of oliguria. The pathogenesis of septic AKI is multifactorial, involving endothelial dysfunction [2], mitochondrial dysfunction [3, 4], tubular mitophagy [5], renal microcirculatory disturbances, amplified inflammatory responses, and disordered energy metabolism [6]. Effective targeted therapies remain limited. Therefore, elucidating the mechanisms of septic AKI is essential for developing improved therapeutic strategies.

Ferroptosis is an iron-dependent regulated cell death distinguished from apoptosis, necrosis, and autophagy by intracellular iron accumulation and lipid peroxidation, exhibiting distinct morphological, biochemical, and genetic features [7]. Glutathione peroxidase 4 (Gpx4) and acyl-CoA synthetase long-chain family member 4 (Acsl4) are pivotal regulators of ferroptosis. Gpx4 suppresses ferroptosis by using glutathione (GSH) to detoxify lipid hydroperoxides and

https://doi.org/10.62347/KAGB1542

maintain redox homeostasis. In contrast, Acsl4 promotes arachidonic acid (AA) and adrenic acid (AdA) into phosphatidylethanolamine (PE), generating polyunsaturated phospholipid substrates for lipid peroxidation [8, 9]. Ferroptosis has been documented in experimental models of septic AKI [10, 11].

Cinnamaldehyde (CA) is a natural aromatic aldehyde derived from multiple parts (leaves, bark, roots, and flowers) of *Cinnamomum* species. CA exhibits antioxidant, antimicrobial, antidiabetic, anti-obesity, and anticancer activities [12], and confers renoprotection in models of ischemia/reperfusion injury [13], cisplatin-induced nephrotoxicity [14], lipopolysaccharide (LPS)-induced renal inflammation [15] and diabetic nephropathy [16]. Notably, CA attenuates doxorubicin-induced cardiotoxicity by suppressing ferroptosis in cardiomyocytes [17]. These findings suggest that CA may modulate ferroptosis in septic AKI, yet its renal mechanisms remain insufficiently defined. Here, we provide evidence of CA's protective effects against LPS-induced renal damage. Integrated network pharmacology, molecular docking, and experimental validation identified glycogen synthase kinase 3 beta (Gsk3β) as a potential key target in septic AKI. Furthermore, our data indicate that CA regulates ferroptosis via the Gsk3β/nuclear factor erythroid 2-related factor 2 (Nrf2)/Kelch-like ECH-associated protein 1 (KEAP1) pathway, offering mechanistic insight and a rationale for targeting this axis.

Materials and methods

Collection of candidate genes associated with septic AKI

We retrieved candidate genes using the keyword "Septic AKI" from various databases and complied the non-redundant results into an Excel file (Disease.xlsx). Specifically, we queried the following resources: (1) PharmGkb (https://www.pharmgkb.org/): a filtering criterion was applied (reported as "Score_gda > 0.1"; please verify this field, as Score_gda typically refers to the DisGeNET GDA score). (2) GeneCards (https://www.genecards.org/): genes with a GeneCards Relevance score > 10 were retained. (3) OMIM (https://omim.org/): disease entries related to sepsis and acute kidney injury were manually screened to extract reported associated genes.

Detailed viral delivery protocol

For in vivo overexpression of Gsk3β, a recombinant lentivirus encoding mouse Gsk3β (GeneChem, Shanghai, China) was used. Eight-week-old male C57BL/6 mice were randomly assigned to experimental groups. Mice in the Gsk3β overexpression (OVE) group received a single tail vein injection of 1 × 10^8 transducing units (TU) of Gsk3β-expressing lentivirus in 100 μL sterile phosphate-buffered saline (PBS), as previously described [PMID: 39472663]. Control mice received the same volume of control lentivirus (empty vector) or PBS. The injection was performed three days prior to LPS administration to ensure efficient transgene expression. Successful overexpression of Gsk3β in renal tissue was confirmed by qPCR and Western blot analysis.

Protein-protein interaction (PPI) network construction and analysis

To delve deeper into the interplay between CA and septic AKI-associated targets, we intersected the curated CA-related targets with the septic AKI by intersecting CA-related genes with those linked to septic AKI. We then imported the shared target dataset into the STRING database (https://string-db.org/), specifying Mus musculus as the species and a minimum required interaction score of 0.4. Subsequently, we downloaded the "string_interactions_short.tsv" file and imported it into Cytoscape 3.7.2 for network visualization, utilizing the string_interactions_short.tsv plugin. Network topology metrics were computed using the CytoNCA plugin to prioritize hub genes, and connected modules were identified with MCODE module for network cluster identification and analysis.

Molecular docking analysis

To assess the binding affinity of key network hubs, molecular docking analysis was employed. The three-dimensional (3D) structures of Gsk3β and CA were retrieved from the RCSB Protein Data Bank (http://www.rcsb.org/). These structures were prepared using the MGLTools_win32_1.5.6 software and stored in PDBQT format. Subsequently, AutoDock Vina 1.1.2 (http://vina.scripps.edu/) was used to evaluate the docking affinity between CA and the target proteins. Finally, the results of the

molecular docking analysis were visually represented using PyMOL software.

Animal experiments

Eight-week-old male C57BL/6 mice were obtained from the Experimental Animal Center of the Institute of Medicine, Shanghai university, and all animal experiments were approved by the Animal Care Committee of Shanghai University and conducted in accordance with the Guide for the Care and Use of Laboratory Animals (Approval No. YS 2024-131). In the initial experiment, the mice were randomly assigned to four groups: a control group (n = 6), an LPS group (10 mg/kg; n = 6), a CA group (40 mg/kg CA; n = 6), and a CA + LPS group (n = 6). The CA dosage was determined based on previous sepsis studies [13]. CA was administered via the tail vein three days prior to LPS injection. After 24 hours, hearts and blood samples were collected. In the subsequent experiment, mice were again randomly distributed into four groups: a control group (n = 6), an LPS group (n = 6), a CA + LPS group (n = 6), and a CA + LPS + Gsk3β OVE group (n = 6).

Animal care and surgical procedures

C57BL/6 mice (8-10 weeks, 20-25 g) were acclimatized ≥ 7 days. Isoflurane anesthesia (3-4% induction; 1.5-2% maintenance) was delivered to the animals on a warming pad with ocular lubrication. Buprenorphine (0.05 mg/kg, s.c.) was given 30 min pre-incision and every 8-12 h for 48 h postoperatively (± meloxicam 1-2 mg/kg every 24 h for 2 days); rescue criteria were predefined. Vital signs and reflex monitoring plus core temperature (36.5-37.5°C) were maintained intraoperatively; postoperative checks followed an intensified schedule during the first 48 h. Humane endpoints (> 20% weight loss, anorexia, severe respiratory distress, moribund state) triggered euthanasia. Euthanasia consisted of slow onset of CO_2 exposure, with a secondary confirmatory method; pentobarbital overdose (150-200 mg/kg, i.p.) was applied for sensitive tissue collection. Procedures complied with AVMA (2020), IACUC, and ARRIVE 2.0 guidelines.

Cell culture and treatment

HK-2 cells (ATCC, Manassas, VA, USA) were cultured in DMEM containing 10% fetal bovine serum (FBS) sourced from Gibco (USA). These cells were maintained in a controlled environment, specifically a humidified atmosphere set at 37°C with 5% CO_2. To induce an inflammatory response in the HK-2 cells, they were stimulated with LPS at a concentration of 10 μM.

CCK-8 assays

HK-2 cells were dissociated into a single-cell suspension using trypsin (Gibco, USA). Subsequently, these cells were seeded into 96-well plates at a density of 2×10^3 cells per well. After treatment, the CCK-8 reagent (Beyotime, China) was diluted with the culture medium and added to the wells. The cells were then incubated for 1 h in a suitable incubator. Finally, the absorbance of these cells was measured using a spectrophotometer from Beckman (USA).

Serum index detection

Utilizing ELISA kits (Shanghai Westang Bio-Tech Co., Ltd., China), we measured the concentrations of IL-6, IL-1β, TNF-α, and MCP-1 in serum samples, as well as MDA and iron levels in kidney tissue.

Lipid peroxidation assay

A lipid peroxidation assay kit (A106, Jiancheng, China) was used to measure LPO levels in kidney tissue lysates according to the manufacturer's instructions. Briefly, the lipid peroxides react with chromogenic agents at 45°C for 60 minutes, yielding a stable chromophore with maximal absorbance at 586 nm [18-20].

Real-time qRT-PCR

Total RNA was extracted (TRIzol, Invitrogen) and reverse-transcribed using SuperScript reverse transcriptase and olig(dT) primers. For quantitative real-time PCR, a CFX Connect detection system from Bio-Rad Laboratories was employed. The primer sequences for Gsk3β, KIM1, and NGAL were designed as follows: sense primer for Gsk3β: 5'-CAAACTACCAAATGGGCGAGACAC-3', antisense primer: 5'-TGAGGCTGCTGTGGCGTTG-3'; sense primer for KIM1: 5'-CCCTGCTGCTACTGCTCCTTG-3', antisense primer: 5'-ACCACGCTTAGAGATGCTGACTTC-3'; sense primer for NGAL: 5'-ACCACGGACTACAACCAGTTCG-3', antisense primer: 5'-CTTGGCAAAGCGGGTGAAACG-3'. The PCR conditions were set at an annealing temperature of 60°C for 40 cycles.

The relative gene expression was calculated using the comparative Ct (threshold cycle) method with the arithmetic formula $2^{-\Delta\Delta}$Ct, and the mRNA level was normalized against β-actin expression.

Western blot analysis

Kidney tissue was lysed in cold RIPA buffer (Beyotime, China) supplemented with Protease Inhibitor Cocktail (Roche, Germany). The isolated proteins underwent a concentration analysis using BCA assays. Subsequently, SDS-PAGE (10%) was performed to separate the proteins, followed by their transfer onto PVDF membranes. The membranes were blocked with TBS-dissolved nonfat dry milk and then incubated overnight at 4°C with a primary antibody dilution buffer (Beyotime, China) containing specific antibodies for Gsk3β (1:1000, cat. no. sc-377213; Santa Cruz Biotechnology, Inc.), Gpx4 (1:1000, cat. no. 52455S; Cell Signaling Technology, Inc.), Acsl4 (1:1000, cat. no. sc-271800; Santa Cruz Biotechnology, Inc.), KIM1 (1:1000, cat. no. 30948-1-AP; Proteintech, Inc.), NGAL (1:1000, cat. no. 26991-1-AP; Proteintech, Inc.) and β-actin (1:1000, cat. no. sc-81178; Santa Cruz Biotechnology, Inc.). After incubation, the membranes were exposed to a horseradish peroxidase-conjugated secondary antibody (1:3000) for 1 hour at room temperature. Finally, the Enhanced Chemiluminescence (ECL) Western Blotting Detection system (Santa Cruz Biotechnology, Inc.) and a GeneGlome HR scanner (SynGene Europe) were employed to visualize the immunoreactive proteins and detect the chemiluminescent signals.

Immunofluorescence analysis

Renal tissue paraffin sections (5 μm) underwent rehydration and were processed in a citric acid buffer via a microwave to facilitate antigen retrieval. Following a 1-hour incubation with 10% BSA, the sections were incubated overnight at 4°C with a primary antibody against Gpx4 (1:1000, cat. no. 52455S; Cell Signaling Technology, Inc.) or Nrf2 (1:1000, cat. no. 16396-1-AP; Proteintech, Inc.). After thorough washing, the sections were incubated with Alexa Fluor 568-conjugated anti-rabbit IgG (Invitrogen, Carlsbad, CA) at 1:400 for 1 h at 37°C in the dark. Nuclei were subsequently counterstained with DAPI (Sigma-Aldrich). The investigator was blinded to group allocation.

Renal tubular injury scores

The assessment of renal tubular injury scores was conducted in a blinded manner. Specifically, two independent pathologists evaluated the renal tubular damage without knowledge of the groupings. These scores were determined on a 0 to 4 scale, where 0 represented no damage (0%), 1 indicated damage affecting less than 25%, 2 corresponded to damage between 26% and 50%, 3 signified damage between 51% and 75%, and 4 denoted damage exceeding 76% [21].

Statistical analysis

Data are presented as mean ± SD, and statistical analysis was conducted using SPSS 16.0 software. For comparing two groups, a two-tailed Student's t-test was employed. When comparing multiple groups, either a one-way or two-way ANOVA, followed by Bonferroni's post-hoc test, was applied. A *p*-value less than 0.05 was deemed to indicate a statistically significant difference.

Results

Identification of CA as a candidate therapeutic agent against LPS-induced injury in HK-2 cells

To identify the therapeutic target for proximal tubule epithelial cell injury triggered by LPS, we conducted a meticulous screen of a small library of natural products from Selleck Chemicals, encompassing 100 compounds as shown in **Figure 1**, using HK-2 cells exposed to LPS. We evaluated cell viability in epithelial cells after treating them with 10 μM LPS for 24 hours, both in the absence and presence of 10 μM of each natural product compound. Out of the 100 compounds tested, CA produced the greatest increase in cell viability against LPS-induced cell injury in HK-2 cells, as shown in **Figure 1**. Furthermore, our results demonstrated that CA attenuated LPS-induced cell injury (**Figure 2A**) and inflammation in a dose-dependent manner (both $P < 0.01$) (**Figure 2B-E**). These findings indicate that CA is a promising therapeutic agent for addressing LPS-induced HK-2 cell injury.

CA attenuates LPS-induced septic AKI

To validate the therapeutic effectiveness of CA in treating septic AKI, in vivo animal studies were undertaken with 2.5, 10 and 40 mg/kg.

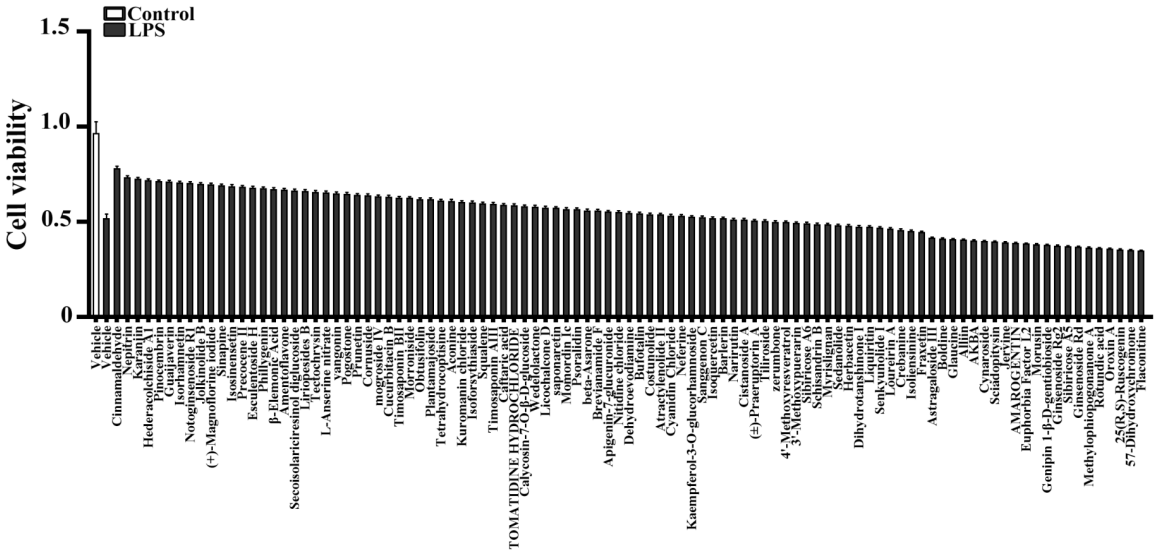

Figure 1. Anti-damage activity of natural products in lipopolysaccharide (LPS)-treated epithelial cells. The HK-2 cells were subjected to LPS (10 μM), both in isolation and in combination with the specified natural product compounds (10 μM). Subsequently, the CCK-8 kit was employed to assess the viability of the cells.

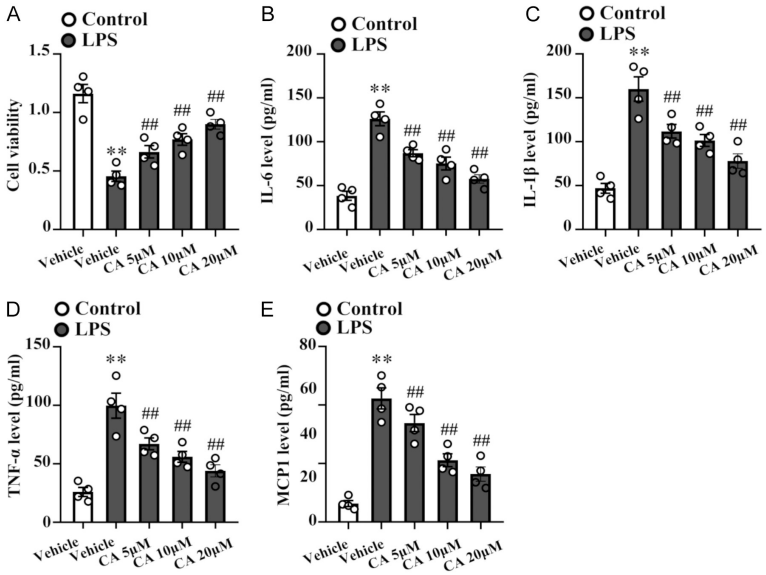

Figure 2. Anti-damage and anti-inflammation activity of cinnamaldehyde (CA) in LPS-treated HK-2 cells. The HK-2 cells were subjected to LPS (10 μM) followed by CA (5, 10 and 20 μM). (A) CCK-8 kit was employed to assess the viability of the cells. (B-E) ELISA was carried out to determine the concentrations of the inflammatory markers. The figure shows the serum levels of Interleukin-6 (IL-6) (B), Interleukin-1β (IL-1β) (C), Tumor necrosis factor-α (TNF-α) (D) and Monocyte chemoattractant protein 1 (MCP1) (E). Data are shown as the mean ± SD (n = 4). $^{**}P < 0.01$ vs. control + vehicle; $^{\#\#}P < 0.01$ vs. LPS + vehicle.

Our findings, depicted in **Figure 3A** and **3B**, indicate that mice undergoing LPS exhibited increased serum levels of creatinine and Bun (both $P < 0.01$). However, these elevations were significantly lowered in mice treated with CA in a dose-responsive fashion. Next, we applied a dose of 40 mg/kg to further investigation. It was found that mice with septic AKI demonstrated a substantial rise in kidney KIM1 and NGAL mRNA and protein levels compared to controls. This surge was notably reversed with CA treatment (both $P < 0.01$) (**Figure 4A-E**). Histological assessments revealed that CA effectively alleviated abnormal tubular damage, specifically manifesting in the reduction of cellular detachment from tubular basement membranes and the accumulation of inflammatory cells, as well as enhanced restoration of brush border integrity (**Figure 4F** and **4G**).

CA mitigates LPS-induced kidney inflammation

To further clarify the impact of CA on LPS-triggered kidney inflammation, the serum concentrations of IL-6, IL-1β, TNF-α, and MCP-1 were carefully measured. As shown in **Figure 5**, Post-LPS injection, mice exhibiting septic AKI demonstrated a marked elevation in the serum levels of IL-6 ($P < 0.01$) (**Figure 5A**), IL-1β ($P <$

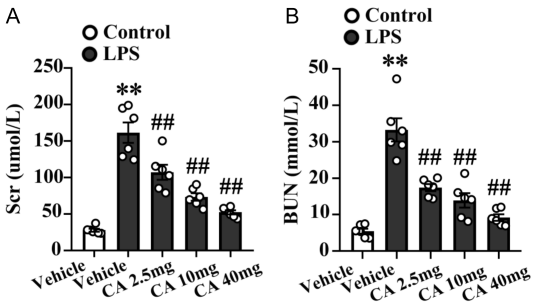

Figure 3. CA reduced serum creatinine and Bun level in a mouse model of LPS-induced AKI in a dose-dependent manner. Mice received LPS (i.p., 10 mg/kg) to induce septic AKI. CA (2.5, 10, 40 mg/kg) was administered via the tail vein, three days prior to LPS injection. The control mice received an equivalent volume of vehicle. All the mice were euthanized 24 h after LPS administration, and blood was collected for serum creatinine (Scr) and Bun detection. A and B. ELISA was carried out to determine Scr and Bun levels. Data are shown as the mean ± SD (n = 6). $^{**}P < 0.01$ vs. control + vehicle; $^{\#\#}P < 0.01$ vs. LPS + vehicle.

0.01) (**Figure 5B**), TNF-α (P < 0.01) (**Figure 5C**), and MCP-1 (P < 0.01) (**Figure 5D**). However, the elevation in these serum markers was partially mitigated by CA, indicating its potential protective effect against LPS-induced kidney inflammation.

CA mitigates LPS-induced kidney ferroptosis

A growing body of research has established a link between septic AKI and ferroptosis. Subsequently, the question arises whether CA can attenuate septic AKI by modulating ferroptosis. In the LPS-induced AKI model, LPS markedly increased renal oxidative/ferroptotic injury, evidenced by elevated malondialdehyde, lipid peroxidation, and renal iron content compared with Control. Administration of the ferroptosis inhibitor ferrostatin-1 (Fer-1) significantly attenuated these increases, lowering malondialdehyde, lipid peroxidation, and iron toward Control levels vs. LPS (Supplementary Figure 2). As illustrated in the **Figure 6A-C**, sepsis mice exhibited significantly elevated levels of malondialdehyde (MDA), iron and LPO in kidney tissue, which were notably reduced following CA administration (both P < 0.01). Additionally, the expression of the ferroptosis-associated protein Gpx4 was significantly downregulated, while the expression of Acsl4 protein was upregulated in kidney tissue from LPS-treated mice (P < 0.01) (**Figure 6D**). CA administration effectively mitigated the sepsis-induced abnormal expression of Gpx4 and Acsl4. Moreover, immunofluorescence analysis of Gpx4 in kidney tissue revealed that CA significantly mitigated the decrease in Gpx4 expression observed in septic kidney tissue (P < 0.01) (**Figure 6E**), indicating that CA's protective effect against septic AKI might be mediated through the suppression of ferroptosis.

Network pharmacology and molecular docking identify GSK3β as a core target of CA in septic AKI

To explore the underlying mechanism of CA against LPS-induced AKI, we performed network pharmacology analysis. A total of 2,879 sepsis-associated AKI-related genes were obtained from DisGeNET database, Genecards database and OMIM database (**Figure 7A**). The CA-related genes and septic AKI genes were intersected to obtain 41 candidate genes for CA against sepsis-induced AKI, for instance Malt, Ptpn22, Brd4, Tlr4, Rela, Nos2, Nos3 Gsk3β, Parp1, Mapk8, Mcl1, etc. PPI analysis demonstrated that Tlr4, Gsk3β, Rela, Mapk8, Mcl1, Nos3 and Parp1 might be the core target (**Figure 7B**). Next, qPCR was conducted to examine the mRNA levels of the above targets. As shown in **Figure 7C**, the mRNA levels of Tlr4, Gsk3β, Rela, Mapk8 and Mcl1 was dramatically increased, whereas the expression of Parp1 and Nos3 in mRNA was dramatically decreased (both P < 0.01). Notably, Gsk3β had the most significant change in expression among them. Molecular docking also verified the affinity between CA and Gsk3β, and the binding energy was -7.0 kcal/mol (**Figure 7D**). Gene Ontology (GO) and Kyoto Encyclopedia of Genes and Genomes (KEGG) enrichment analyses revealed various pathways associated with septic AKI, including the PI3K-Akt pathway, IL-17 pathway, and Hif1 pathway (**Figure 7E** and **7F**). These findings suggested that these pathways might be involved in the renoprotective effects of CA against septic AKI.

CA mitigates LPS-induced renal inflammation and injury partly via GSK3β modulation

To delve deeper into the role of Gsk3β in CA's protective mechanism against septic AKI, we conducted a meticulous measurement of Gsk3β expression at the protein level. Our findings revealed that LPS-treated kidney tissue

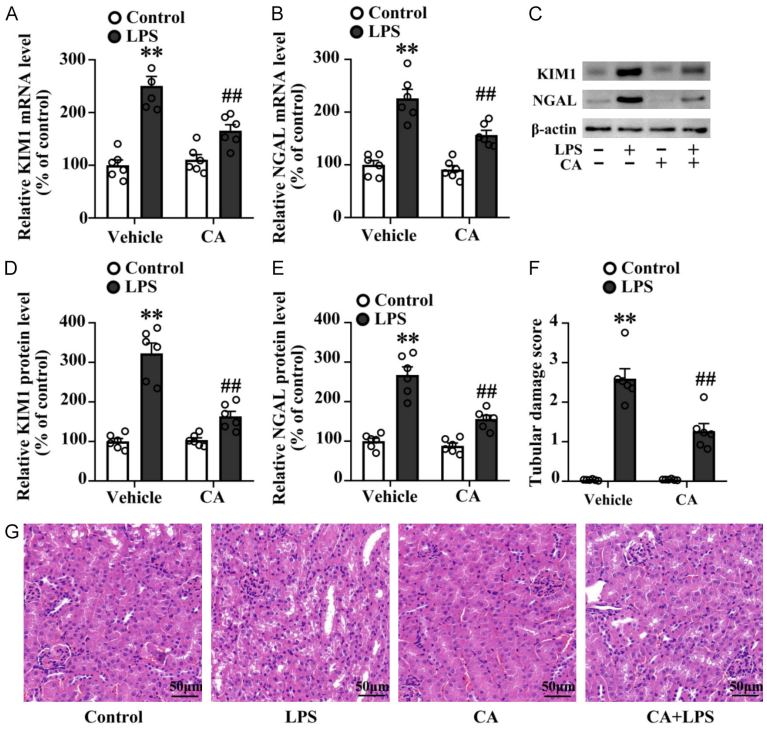

Figure 4. CA mitigates LPS-induced AKI. Mice received LPS (i.p., 10 mg/kg) and CA (i.v., 40 mg/kg), and CA administration was carried out three days prior to LPS injection. The control mice received an equivalent volume of vehicle. All the mice were euthanized 24 h after LPS administration, and blood was collected for serum creatinine (Scr) and Bun detection. A-E. qPCR and western blot analysis were carried out to determine the mRNA and protein levels of KIM1 and NGAL in kidney tissues. F and G. HE staining was performed to detect histological changes in the kidney and tubular damage was quantified. Scale bar = 50 μm. Data are shown as the mean ± SD (n = 6). $^{**}P < 0.01$ vs. control + vehicle; $^{\#\#}P < 0.01$ vs. LPS + vehicle.

exhibited a marked elevation in Gsk3β protein levels ($P < 0.01$). However, CA administration significantly mitigated this increase ($P < 0.01$) (**Figure 8A**). To further investigate the impact of Gsk3β overexpression (OVE) on septic AKI and inflammation, we employed a Gsk3β lentivirus. As shown in Supplementary Figure 1A and 1B, the lentiviral delivery of Gsk3β resulted in a significant, approximately 4.30 ± 0.75-fold increase in Gsk3β expression within the kidney tissue of Gsk3β OVE mice, as compared to control animals. Furthermore, immunofluorescence staining specifically targeting Gsk3β revealed an elevated level of Gsk3β in both the glomerular and interstitial regions of the kidney in Gsk3β OVE mice, in contrast to the controls. In addition, Gsk3β OVE negated the protective effects of CA against LPS-induced renal injury. This was evidenced by re-elevated serum creatinine and Bun, as well as increased renal KIM1 and NGAL expression at the mRNA and protein levels (both $P < 0.01$) (**Figure 8B-H**). Histological analysis also corroborated these findings, demonstrating that Gsk3β OVE abolished CA's positive impact on LPS-mediated tubular structural abnormalities (**Figure 8I** and **8J**).

ELISA revealed that Gsk3β OVE abrogated CA's inhibitory effect on LPS-induced inflammatory responses. This was characterized by a surge in the levels of IL-6, IL-1β, TNF-α, and MCP-1 (both $P < 0.01$) (**Figure 9A-D**). These findings provide valuable insights into the intricate interplay between Gsk3β, CA, and septic AKI, highlighting the potential therapeutic implications of targeting Gsk3β in the management of this condition.

CA inhibited LPS-induced renal ferroptosis via the Gsk3β/Nrf2/Keap1 pathway

Subsequently, we investigated the influence of Gsk3β OVE on CA's protective effect against LPS-induced kidney ferroptosis. Our findings, illustrated in the accompanying **Figure 10A-D**, demonstrate that Gsk3β OVE hinders CA's ability to protect against LPS-induced renal ferroptosis. This was evident from the elevated levels of renal MDA ($P < 0.01$) (**Figure 10A**), iron ($P < 0.01$) (**Figure 10B**), LPO ($P < 0.01$) (**Figure 10C**) and Acsl4 protein, coupled with a decrease in Gpx4 levels ($P < 0.01$) (**Figure 10D**), suggesting that CA attenuated LPS-induced renal ferroptosis by regulating the expression of Gsk3β. Immunofluorescence analysis demonstrated that the upregulation effect of CA on Gpx4 expression in septic kidney tissue was mitigated by Gsk3β OVE (**Figure 10E**). Prior research has firmly established that the involvement of Gsk3β in modulating the Nrf2/Gpx4 pathway can potentially impact the progression of ferroptosis [22-24]. Western blot analysis was employed to assess the protein expression level of Nrf2 and Keap1. In the LPS group, there was a notable decrease in the protein levels of

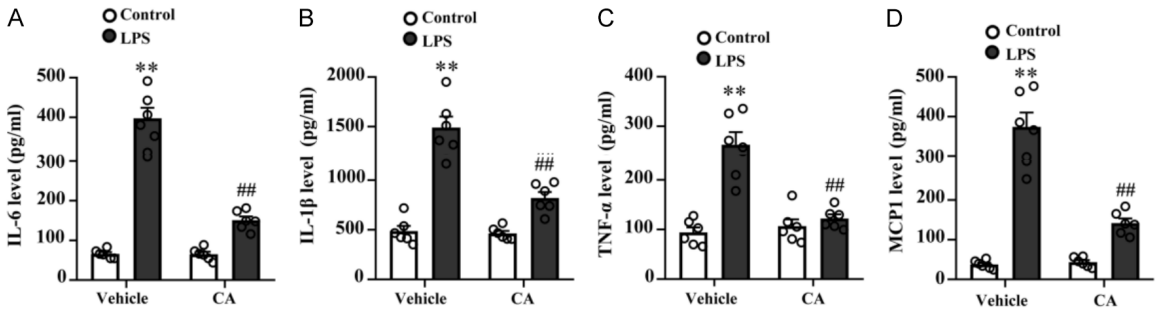

Figure 5. CA mitigates LPS-induced inflammatory responses. ELISA was carried out to determine the concentrations of the inflammatory markers. The figure shows the serum levels of IL-6 (A), IL-1β (B), TNF-α (C) and MCP-1 (D). Data are shown as the mean ± SD (n = 6). $^{**}P < 0.01$ vs. control + vehicle; $^{\#\#}P < 0.01$ vs. LPS + vehicle.

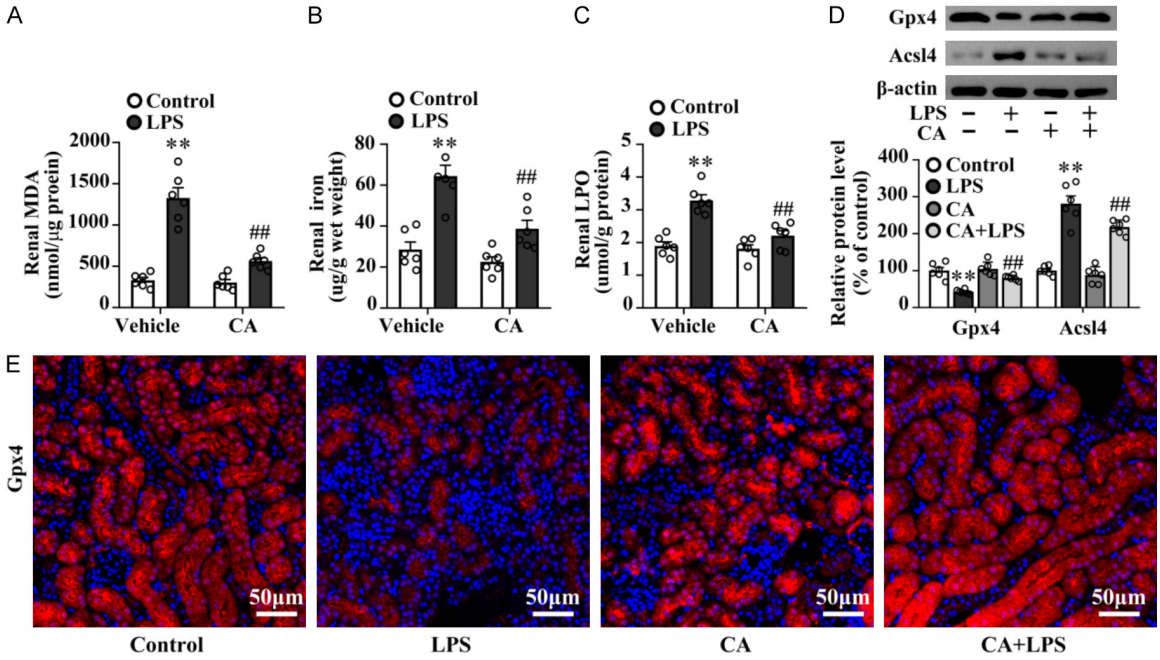

Figure 6. CA mitigates LPSinduced renal ferroptosis. (A and B) ELISA was carried out to determine the concentrations of the ferroptosis markers. The figure shows the renal levels of MDA (A) and iron (B). (C) Renal LPO level. (D) Western blot analysis was carried out to determine the protein levels of Gpx4 and Acsl4. (E) Immunofluorescent staining of Gpx4. Nuclei were counterstained with DAPI (blue). Data are shown as the mean ± SD (n = 6). $^{**}P < 0.01$ vs. control + vehicle; $^{\#\#}P < 0.01$ vs. LPS + vehicle.

Nrf2 and a significant increase in Keap1 levels ($P < 0.01$). However, the administration of CA reversed these alterations in Nrf2 and Keap1 protein levels ($P < 0.01$). Interestingly, the inhibitory effect of CA on these changes was abrogated by Gsk3β overexpression (lentiviral delivery) ($P < 0.01$) (**Figure 10F**). Immunofluroscence staining also indicated that CA could significantly reverse the LPS-induced decrease in Nrf2 expression in the kidney (**Figure 10G**). These results suggest that Gsk3β/Nrf2/Keap1 pathway is involved in the impact of CA against LPS caused renal ferroptosis.

Discussion

CA, an active constituent of cinnamon, has long been used as a natural flavor and aroma agent in both culinary and industrial applications. Moreover, CA has been extensively utilized in biological research as a promising therapeutic agent for treating various diseases due to its diverse therapeutic properties, encompassing antioxidant, anti-inflammatory, anti-apoptotic, antimicrobial, anti-diabetic, anti-obesity, and anti-cancer effects [12, 25]. Currently, a growing body of evidence suggests that CA offers

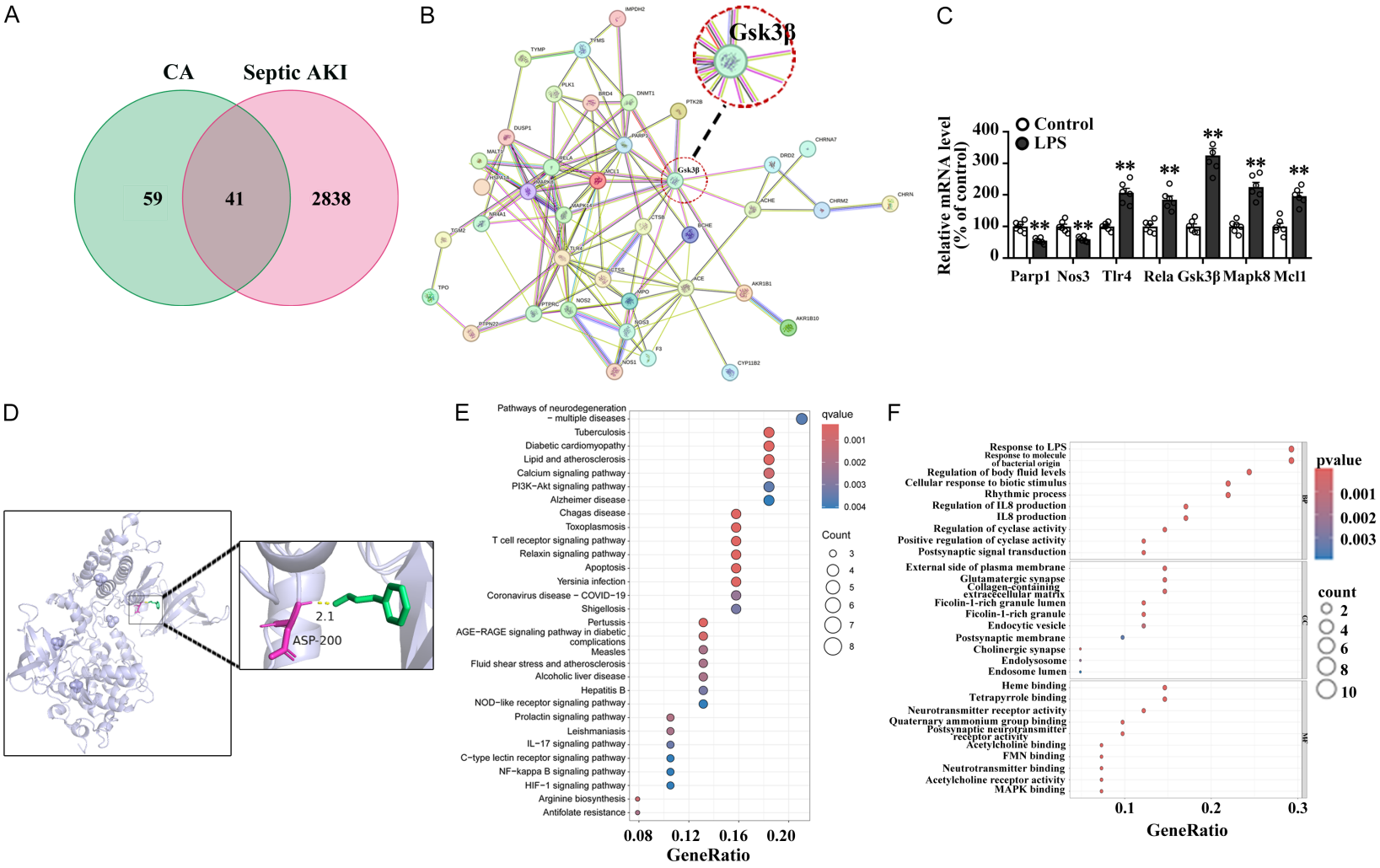

Figure 7. Glycogen synthase kinase-3β (Gsk3β) might be the potential target of CA in septic AKI. A. Venn diagram analysis of CA and SIC. B. Core target network. C. qPCR analysis was carried out to determine the mRNA levels of Parp1, Nos3, Tlr4, Rela, Gsk3β, Mapk8 and Mcl1 in kidney tissues. D. Molecular docking visualization of Gsk3β-CA. E. KEGG analysis. F. GO analysis. Data are shown as the mean ± SD (n = 6). $^{**}P < 0.01$ vs. control.

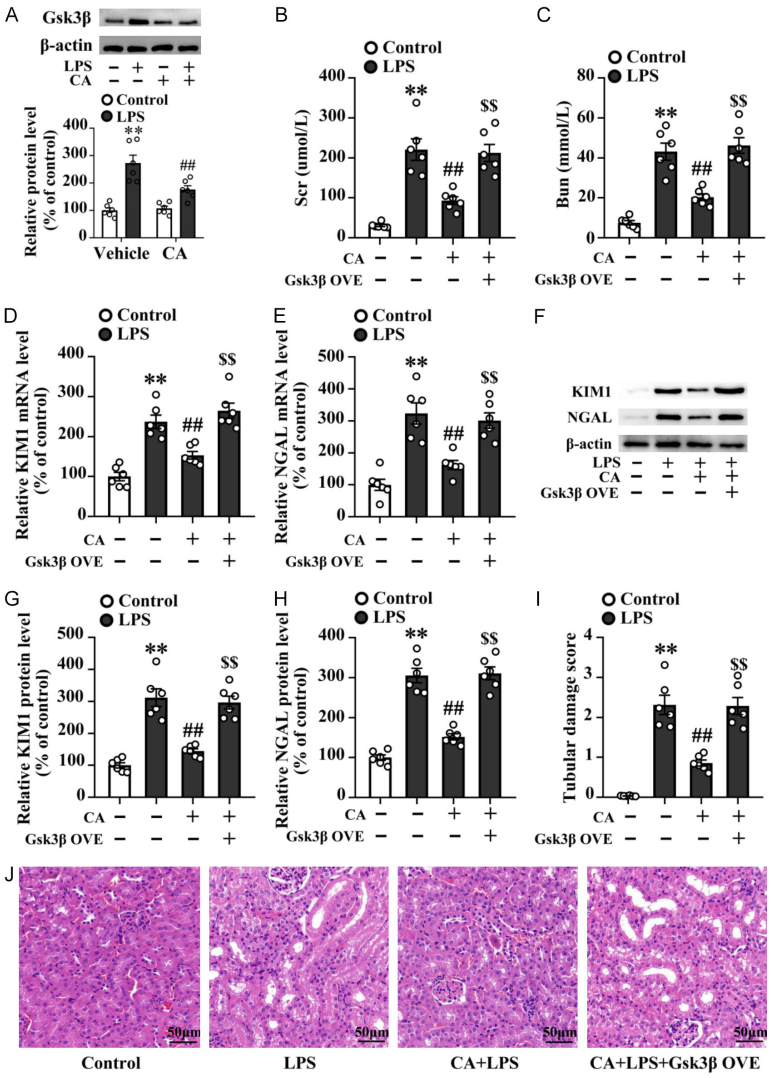

Figure 8. Gsk3β OVE blocked the protective role of CA against LPS-induced AKI. (A) Western blot analysis was carried out to determine the protein levels of Gsk3β in LPS-treated kidney tissue with or without CA administration. (B-G) Adenovirus particles containing Gsk3β or control vector were administered to mice by intra-parenchymal injection. One week after intra-parenchymal injection, mice were subjected to LPS (i.p., 10 mg/kg) and CA (i.v., 40 mg/kg), and CA administration was carried out three days prior to LPS injection. The control mice received an equivalent volume of vehicle. (B and C) The figure shows the serum levels of creatinine (B) and Bun (C). (D-H) qPCR and western blot analysis was carried out to determine the mRNA and protein levels of KIM1 and NGAL in kidney tissues. (I and J) HE staining was performed to detect histological changes in the kidney and tubular damage was quantified. Scale bar = 50 μm. Data are shown as the mean ± SD (n = 6). $^{**}P < 0.01$ vs. control + vehicle; $^{\#\#}P < 0.01$ vs. LPS + vehicle; $^{\$\$}P < 0.01$ vs. CA + LPS.

significant benefits in the treatment of kidney diseases, including diabetic nephropathy [16, 26], kidney senescence [27], cisplatin-induced nephrotoxicity [14], renal cell carcinoma [28] and renal ischemia/reperfusion injury [13]. In the present study, we show that CA protects against LPS-induced septic AKI by suppressing ferroptosis. Network pharmacology plus experimental confirmation identified Gsk3β as a core target of CA in septic AKI. Suppression of Gsk3β was associated with the renoprotective role of CA against septic AKI via modulation of Nrf2/Gpx4 pathway.

Ferroptosis is characterized by increased lipid peroxidation, reactive oxygen species (ROS) overload, and plasma membrane rupture. Until now, there only limited studies have explored the relationship between CA and ferroptosis. In the realm of cancer and bacterial research, CA-based organic ligands [29], nanoparticles [30], and nano-emulsions [31] have been reported to induce ferroptosis through various mechanisms, including blocking the reduction of lipid peroxides, disrupting redox homeostasis, and causing cell membrane disruption, respectively, ultimately exerting a potential role in cancer and antibacterial therapy. Conversely, in cardiovascular research, CA has been reported to alleviate doxorubicin-induced cardiotoxicity by suppressing ferroptosis, achieved through modulating Nrf2 nuclear translocation and HO-1 expression [17]. Consistent with this study, we have also demonstrated the inhibitory effect of CA on ferroptosis in kidney tissue from LPS-treated mice, further highlighting its potential therapeutic role in the management of kidney-related disorders. The diverse impact of CA on ferroptosis may be attributed to the varying microenvironments present in different diseases and tissues.

Gsk3β, a highly conserved serine/threonine protein kinase, regulates cell proliferation, differentiation, apoptosis, and necrosis, underscoring its pivotal role in cellular homeostasis

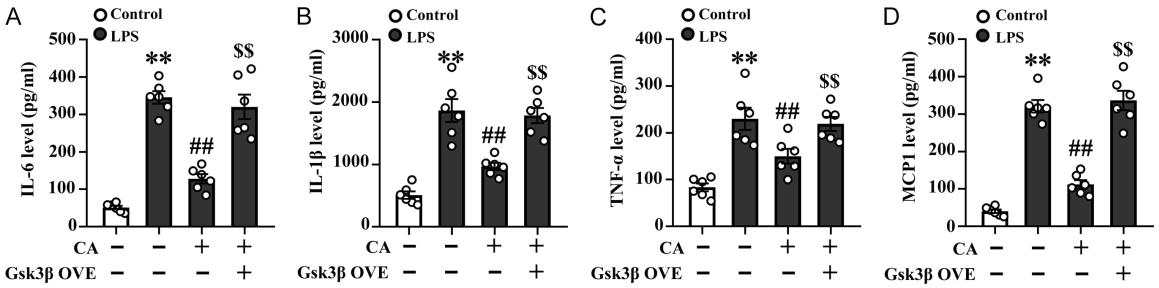

Figure 9. Gsk3β OVE blocked the protective role of CA against LPS-induced inflammatory responses. ELISA was carried out to determine the concentrations of the inflammatory markers. The figure shows the serum levels of IL-6 (A), IL-1β (B), TNF-α (C) and MCP-1 (D). Data are shown as the mean ± SD (n = 6). **P < 0.01 vs. control + vehicle; $^{\#\#}$P < 0.01 vs. LPS + vehicle; $^{\$\$}$P < 0.01 vs. CA + LPS.

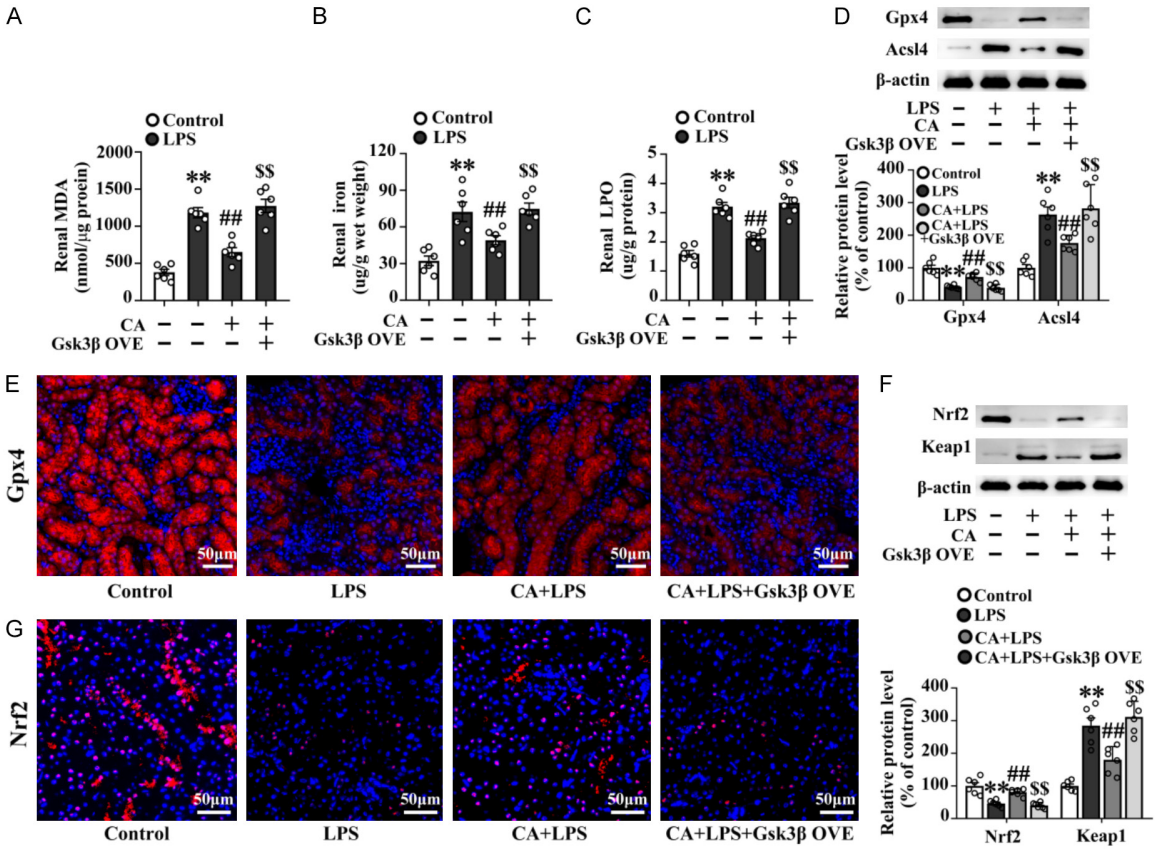

Figure 10. Gsk3β OVE blocked the protective role of CA against LPS-induced renal ferroptosis. (A and B) ELISA was carried out to determine the concentrations of the ferroptosis markers. The figure shows the renal levels of MDA (A) and iron (B). (C) Renal LPO level. (D) Western blot analysis was carried out to determine the protein levels of Gpx4 and Acsl4. (E) Immunofluorescent staining of Gpx4. Nuclei were counterstained with DAPI (blue). (F) Western blot analysis was carried out to determine the protein levels of Nrf2 and Keap1. (G) Immunofluorescent staining of Nrf2. Nuclei were counterstained with DAPI (blue). Scale bar = 50 μm. Data are shown as the mean ± SD (n = 6). **P < 0.01 vs. control + vehicle; $^{\#\#}$P < 0.01 vs. LPS + vehicle.

and biological processes [32]. As a highly expressed kinase in kidney tissue, Gsk3β plays a pivotal role in nephropathy, particularly in AKI, that is broadly acknowledged. Among these, a novel Gsk3β inhibitor, 5n, was reported to attenuate cisplatin induced AKI through a PP2Ac-dependent mechanisms [33]. Other Gsk3β inhibitors, TDZD-8 and lithium, have been documented to exhibit protective effects against renal ischemia-reperfusion injury and

nonsteroidal anti-inflammatory drugs (NSAIDs) or rhabdomyolysis-associated AKI [32, 34, 35]. More importantly, Howard et al. showed that both pharmacological inhibition by TDZD-8 and proximal tubule-specific deletion of Gsk3β confers protection against HgCl2-induced AKI in mice [36].

Recently, Gsk3β has emerged as a crucial modulator that enhances ferroptosis. Both the selective inhibitor LY2090314 and Gsk3β knockdown have been shown to mitigate ferroptosis. Furthermore, Gsk3β knockdown can decrease the expression of iron metabolic components, disrupting iron homeostasis and reducing intracellular labile iron levels [37]. Recent research has illuminated the intricate interplay between Gsk3β, Nrf2, and Gpx4. Gsk-3β acts as a negative regulator of Nrf2 and a common effector of numerous Nrf2 inducers in the non-canonical, Keap1-independent pathway [38]. As a versatile serine/threonine kinase, Gsk3β promotes Nrf2 inactivation by retaining Nrf2 within the cytoplasm or facilitating its export [39, 40]. Gsk3β initiates phosphorylation that drives nuclear export of Nrf2, thereby limiting its transcriptional activity [40-43]. Our data indicate that GSK3β overexpression (OVE) blunts the CA-induced increase of Nrf2 in both the cytoplasm and nucleus, implicating the GSK3β/Nrf2 axis in CA's protection against LPS-induced renal ferroptosis. In addition, the activation of the Gsk3β/Nrf2 signaling pathway, leading to the upregulation of Gpx4, has been linked to the anti-ferroptotic effects of various therapeutic agents, including dexmedetomidine, Schizandrin B, and Britanin [24, 40, 44]. One study emphasized balancing the Gsk3β/Nrf2 axis as a strategy to modulate elastin-triggered ferroptosis in breast cancer [22]. In the present study, we found that the inhibition of Gsk3β mediated by CA impedes ferroptosis by upregulating Gpx4, which subsequently attenuates septic AKI. There are a few limitations in this study. A major limitation is that although Nrf2 expression was assessed, the precise intracellular localization of Nrf2, along with the mechanism behind CA's downregulation of Gsk3β, remains elusive.

Conclusions

CA attenuates LPS-induced AKI by inhibiting ferroptosis via the Gsk3β/Nrf2/Gpx4 pathway. Our findings provide a new molecular mechanism for LPS-induced AKI from the perspective of renal ferroptosis and demonstrate the therapeutic potential of CA for LPS-induced AKI through regulation of the Gsk3β/Nrf2/Gpx4/ferroptosis pathway.

Acknowledgements

This work was supported by the PLA Special Fund for Health Care (15BJZ19), Hunan Provincial Natural Science Foundation (2021JJ-31058).

Disclosure of conflict of interest

None.

Address correspondence to: Ye Tian, Department of Anesthesiology, The Sixth Medical Center of Chinese PLA General Hospital, No. 6 Fucheng Road, Beijing 100048, China. E-mail: geshuaina@163.com; Haitao Tian, Department of Geriatric Medicine, The Sixth Medical Center of Chinese PLA General Hospital, No. 6 Fucheng Road, Beijing 100048, China. E-mail: Tianhaitao0039@163.com

References

[1] Bellomo R, Kellum JA and Ronco C. Acute kidney injury. Lancet 2012; 380: 756-766.

[2] Privratsky JR, Ide S, Chen Y, Kitai H, Ren J, Fradin H, Lu X, Souma T and Crowley SD. A macrophage-endothelial immunoregulatory axis ameliorates septic acute kidney injury. Kidney Int 2023; 103: 514-528.

[3] Tsuji N, Tsuji T, Yamashita T, Hayase N, Hu X, Yuen PS and Star RA. BAM15 treats mouse sepsis and kidney injury, linking mortality, mitochondrial DNA, tubule damage, and neutrophils. J Clin Invest 2023; 133: e152401.

[4] Tan Z, Liu Q, Chen H, Zhang Z, Wang Q, Mu Y, Li Y, Hu T, Yang Y and Yan X. Pectolinarigenin alleviated septic acute kidney injury via inhibiting Jak2/Stat3 signaling and mitochondria dysfunction. Biomed Pharmacother 2023; 159: 114286.

[5] Ni Y, Wu GH, Cai JJ, Zhang R, Zheng Y, Liu JQ, Yang XH, Yang X, Shen Y, Lai JM, Ye XM and Mo SJ. Tubule-mitophagic secretion of SerpinG1 reprograms macrophages to instruct anti-septic acute kidney injury efficacy of high-dose ascorbate mediated by NRF2 transactivation. Int J Biol Sci 2022; 18: 5168-5184.

[6] Bellomo R, Kellum JA, Ronco C, Wald R, Martensson J, Maiden M, Bagshaw SM, Glassford NJ, Lankadeva Y, Vaara ST and Schneider A. Acute kidney injury in sepsis. Intensive Care Med 2017; 43: 816-828.

[7] Dixon SJ, Lemberg KM, Lamprecht MR, Skouta R, Zaitsev EM, Gleason CE, Patel DN, Bauer AJ, Cantley AM, Yang WS, Morrison B 3rd and Stockwell BR. Ferroptosis: an iron-dependent form of nonapoptotic cell death. Cell 2012; 149: 1060-1072.

[8] Yang WS, SriRamaratnam R, Welsch ME, Shimada K, Skouta R, Viswanathan VS, Cheah JH, Clemons PA, Shamji AF, Clish CB, Brown LM, Girotti AW, Cornish VW, Schreiber SL and Stockwell BR. Regulation of ferroptotic cancer cell death by GPX4. Cell 2014; 156: 317-331.

[9] Doll S, Proneth B, Tyurina YY, Panzilius E, Kobayashi S, Ingold I, Irmler M, Beckers J, Aichler M, Walch A, Prokisch H, Trümbach D, Mao G, Qu F, Bayir H, Füllekrug J, Scheel CH, Wurst W, Schick JA, Kagan VE, Angeli JP and Conrad M. ACSL4 dictates ferroptosis sensitivity by shaping cellular lipid composition. Nat Chem Biol 2017; 13: 91-98.

[10] Yang Y, Lin Q, Zhu X, Shao X, Li S, Li J, Wu J, Jin H, Qi C, Jiang N, Zhang K, Wang Q, Gu L and Ni Z. Activation of lipophagy is required for RAB7 to regulate ferroptosis in sepsis-induced acute kidney injury. Free Radic Biol Med 2024; 218: 120-131.

[11] Zan H, Liu J, Yang M, Zhao H, Gao C, Dai Y, Wang Z, Liu H and Zhang Y. Melittin alleviates sepsis-induced acute kidney injury by promoting GPX4 expression to inhibit ferroptosis. Redox Rep 2024; 29: 2290864.

[12] Muhoza B, Qi B, Harindintwali JD, Koko MYF, Zhang S and Li Y. Encapsulation of cinnamaldehyde: an insight on delivery systems and food applications. Crit Rev Food Sci Nutr 2023; 63: 2521-2543.

[13] Chen L, Yuan J, Li H, Ding Y, Yang X, Yuan Z, Hu Z, Gao Y, Wang X, Lu H, Cai Y, Bai Y and Pan X. Trans-cinnamaldehyde attenuates renal ischemia/reperfusion injury through suppressing inflammation via JNK/p38 MAPK signaling pathway. Int Immunopharmacol 2023; 118: 110088.

[14] El-Sayed el-SM, Abd El-Raouf OM, Fawzy HM and Manie MF. Comparative study of the possible protective effects of cinnamic acid and cinnamaldehyde on cisplatin-induced nephrotoxicity in rats. J Biochem Mol Toxicol 2013; 27: 508-514.

[15] Ka SM, Kuoping Chao L, Lin JC, Chen ST, Li WT, Lin CN, Cheng JC, Jheng HL, Chen A and Hua KF. A low toxicity synthetic cinnamaldehyde derivative ameliorates renal inflammation in mice by inhibiting NLRP3 inflammasome and its related signaling pathways. Free Radic Biol Med 2016; 91: 10-24.

[16] Huang JS, Lee YH, Chuang LY, Guh JY and Hwang JY. Cinnamaldehyde and nitric oxide attenuate advanced glycation end products-induced the Jak/STAT signaling in human renal tubular cells. J Cell Biochem 2015; 116: 1028-1038.

[17] Mao M, Zheng W, Deng B, Wang Y, Zhou D, Shen L, Niku W and Zhang N. Cinnamaldehyde alleviates doxorubicin-induced cardiotoxicity by decreasing oxidative stress and ferroptosis in cardiomyocytes. PLoS One 2023; 18: e0292124.

[18] Bai T, Li M, Liu Y, Qiao Z and Wang Z. Inhibition of ferroptosis alleviates atherosclerosis through attenuating lipid peroxidation and endothelial dysfunction in mouse aortic endothelial cell. Free Radic Biol Med 2020; 160: 92-102.

[19] Tao WH, Shan XS, Zhang JX, Liu HY, Wang BY, Wei X, Zhang M, Peng K, Ding J, Xu SX, Li LG, Hu JK, Meng XW and Ji FH. Dexmedetomidine attenuates ferroptosis-mediated renal ischemia/reperfusion injury and inflammation by inhibiting ACSL4 via α2-AR. Front Pharmacol 2022; 13: 782466.

[20] Wang D, Liu J, Chen X, Chen J, Zhao T, Du J, Wang C, Meng Q, Sun H, Wang F, Liu K and Wu J. Renal transporter OAT1 and PPAR-α pathway co-contribute to icaritin-induced nephrotoxicity. Phytother Res 2023; 37: 549-562.

[21] Li N, Lin G, Zhang H, Sun J, Gui M, Liu Y, Li W, Zhan Z, Li Y, Pan S, Liu J and Tang J. Lyn attenuates sepsis-associated acute kidney injury by inhibition of phospho-STAT3 and apoptosis. Biochem Pharmacol 2023; 211: 115523.

[22] Wu X, Liu C, Li Z, Gai C, Ding D, Chen W, Hao F and Li W. Regulation of GSK3β/Nrf2 signaling pathway modulated erastin-induced ferroptosis in breast cancer. Mol Cell Biochem 2020; 473: 217-228.

[23] Gui J, Wang L, Liu J, Luo H, Huang D, Yang X, Song H, Han Z, Meng L, Ding R, Yang J and Jiang L. Ambient particulate matter exposure induces ferroptosis in hippocampal cells through the GSK3B/Nrf2/GPX4 pathway. Free Radic Biol Med 2024; 213: 359-370.

[24] Lu H, Xiao H, Dai M, Xue Y and Zhao R. Britanin relieves ferroptosis-mediated myocardial ischaemia/reperfusion damage by upregulating GPX4 through activation of AMPK/GSK3β/Nrf2 signalling. Pharm Biol 2022; 60: 38-45.

[25] Lan H, Zheng Q, Wang K, Li C, Xiong T, Shi J and Dong N. Cinnamaldehyde protects donor heart from cold ischemia-reperfusion injury via the PI3K/AKT/mTOR pathway. Biomed Pharmacother 2023; 165: 114867.

[26] Zhu R, Liu H, Liu C, Wang L, Ma R, Chen B, Li L, Niu J, Fu M, Zhang D and Gao S. Cinnamaldehyde in diabetes: a review of pharmacology, pharmacokinetics and safety. Pharmacol Res 2017; 122: 78-89.

[27] Xiao Q. Cinnamaldehyde attenuates kidney senescence and injury through PI3K/Akt path-

way-mediated autophagy via downregulating miR-155. Ren Fail 2022; 44: 601-614.
[28] Ahn CR, Park J, Kim JE, Ahn KS, Kim YW, Jeong M, Kim HJ, Park SH and Baek SH. Cinnamaldehyde and hyperthermia co-treatment synergistically induces ROS-mediated apoptosis in ACHN renal cell carcinoma cells. Biomedicines 2020; 8: 357.
[29] Zhang Z, Pan Y, Cun JE, Li J, Guo Z, Pan Q, Gao W, Pu Y, Luo K and He B. A reactive oxygen species-replenishing coordination polymer nanomedicine disrupts redox homeostasis and induces concurrent apoptosis-ferroptosis for combinational cancer therapy. Acta Biomater 2022; 151: 480-490.
[30] Yan Z, Wu S, Zhou Y and Li F. Acid-responsive micelles releasing cinnamaldehyde enhance rsl3-induced ferroptosis in tumor cells. ACS Biomater Sci Eng 2022; 8: 2508-2517.
[31] Sun J, Shen QJ, Pan JN, Zheng X, Yu T and Zhou WW. Ferrous sulfate combined with ultrasound emulsified cinnamaldehyde nanoemulsion to cause ferroptosis in Escherichia coli O157:H7. Ultrason Sonochem 2024; 106: 106884.
[32] Liu Q, Kong Y, Guo X, Liang B, Xie H, Hu S, Han M, Zhao X, Feng P, Lyu Q, Dong W, Liang X, Wang W and Li C. GSK-3β inhibitor TDZD-8 prevents reduction of aquaporin-1 expression via activating autophagy under renal ischemia reperfusion injury. FASEB J 2021; 35: e21809.
[33] Cai YT, Li Z, Wang YY, Li C and Ma QY. A novel GSK3β inhibitor 5n attenuates acute kidney injury. Heliyon 2024; 10: e29159.
[34] Bao H, Ge Y, Zhuang S, Dworkin LD, Liu Z and Gong R. Inhibition of glycogen synthase kinase-3β prevents NSAID-induced acute kidney injury. Kidney Int 2012; 81: 662-673.
[35] Shimizu MHM, Volpini RA, de Bragança AC, Nascimento MM, Bernardo DRD, Seguro AC and Canale D. Administration of a single dose of lithium ameliorates rhabdomyolysis-associated acute kidney injury in rats. PLoS One 2023; 18: e0281679.
[36] Howard C, Tao S, Yang HC, Fogo AB, Woodgett JR, Harris RC and Rao R. Specific deletion of glycogen synthase kinase-3β in the renal proximal tubule protects against acute nephrotoxic injury in mice. Kidney Int 2012; 82: 1000-1009.
[37] Wang L, Ouyang S, Li B, Wu H and Wang F. GSK-3β manipulates ferroptosis sensitivity by dominating iron homeostasis. Cell Death Discov 2021; 7: 334.
[38] Luo M, Zheng Y, Tang S, Gu L, Zhu Y, Ying R, Liu Y, Ma J, Guo R, Gao P and Zhang C. Radical oxygen species: an important breakthrough point for botanical drugs to regulate oxidative stress and treat the disorder of glycolipid metabolism. Front Pharmacol 2023; 14: 1166178.
[39] Jain AK and Jaiswal AK. GSK-3beta acts upstream of Fyn kinase in regulation of nuclear export and degradation of NF-E2 related factor 2. J Biol Chem 2007; 282: 16502-16510.
[40] Wang Z, Yao M, Jiang L, Wang L, Yang Y, Wang Q, Qian X, Zhao Y and Qian J. Dexmedetomidine attenuates myocardial ischemia/reperfusion-induced ferroptosis via AMPK/GSK-3β/Nrf2 axis. Biomed Pharmacother 2022; 154: 113572.
[41] Huang W, Wen F, Yang P, Li Y, Li Q and Shu P. Yi-qi-hua-yu-jie-du decoction induces ferroptosis in cisplatin-resistant gastric cancer via the AKT/GSK3β/NRF2/GPX4 axis. Phytomedicine 2024; 123: 155220.
[42] Anzovino A, Chiang S, Brown BE, Hawkins CL, Richardson DR and Huang MLH. Molecular alterations in a mouse cardiac model of friedreich ataxia: an impaired Nrf2 response mediated via upregulation of Keap1 and activation of the Gsk3β axis. Am J Pathol 2017; 187: 2858-2875.
[43] Sanz-Alcázar A, Portillo-Carrasquer M, Delaspre F, Pazos-Gil M, Tamarit J, Ros J and Cabiscol E. Deciphering the ferroptosis pathways in dorsal root ganglia of Friedreich ataxia models. The role of LKB1/AMPK, KEAP1, and GSK3β in the impairment of the NRF2 response. Redox Biol 2024; 76: 103339.
[44] Dong C, Song C, He Z, Song Q, Song T, Liu J, Xiong Y, Su X, Zhou J, Yang S and Liao W. Protective efficacy of Schizandrin B on ameliorating nephrolithiasis via regulating GSK3β/Nrf2 signaling-mediated ferroptosis in vivo and in vitro. Int Immunopharmacol 2023; 117: 110042.

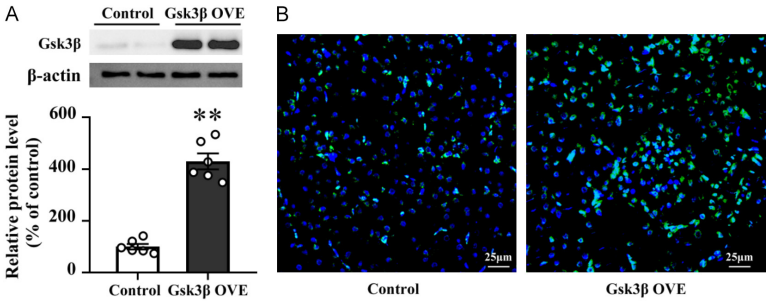

Supplementary Figure 1. Verification of GSK3β overexpression. A. Representative immunoblot showing increased GSK3β protein abundance in the GSK3β overexpression (GSK3β OVE) group versus Control; β-actin serves as a loading control. Right (or below) is densitometric quantification of GSK3β normalized to β-actin and expressed as % of Control (Control set to 100%). B. Representative immunofluorescence (or immunocytochemistry; confirm) images of Control and GSK3β OVE groups demonstrating elevated GSK3β signal intensity; scale bar = 25 μm. Experimental details (vector, transfection or infection method, multiplicity of infection or plasmid amount, exposure time post-transfection, cell type, and antibody sources) are described in Methods. Data are mean ± SD, n = 6 independent experiments (or biological replicates). Statistical analysis: unpaired two-tailed t test if only two groups. Significance: *P < 0.05, **P < 0.01, ***P < 0.001 versus Control.

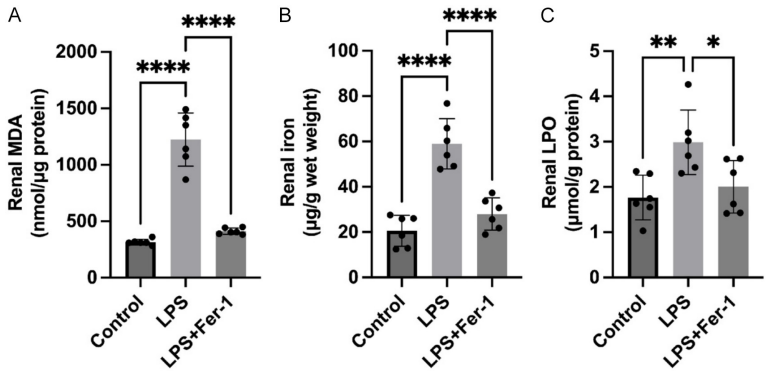

Supplementary Figure 2. Ferrostatin-1 attenuates LPS-induced increases in renal lipid peroxidation and iron accumulation. A. Renal malondialdehyde (MDA) levels (reported in the source file as nmol/μg protein; please verify whether the intended unit is nmol/mg protein). B. Renal lipid peroxidation (LPO) (μmol/g protein). C. Renal iron content (μg/g wet weight). Animals were divided into Control, LPS, and LPS + Fer-1 groups. LPS was administered at 10 mg/kg, and ferrostatin-1 (Fer-1, 10 mg/kg) was given as described in Methods. Data are presented as mean ± SD (n = 6). Statistical analysis: one-way ANOVA with Tukey's post hoc test. Significance indicators: *P < 0.05, **P < 0.01, ***P < 0.001, ****P < 0.0001 (define the comparison basis, e.g. vs. Control unless otherwise indicated). Abbreviations: Fer-1, ferrostatin-1; LPO, lipid peroxidation; MDA, malondialdehyde.